Analytica Chimica Acta 1229 (2022) 340195

Contents lists available at ScienceDirect

Analytica Chimica Acta

journal homepage: www.elsevier.com/locate/aca

Direct determination of free Zn concentration in samples of biological interest

Lucía López-Solís [a], Encarna Companys [a], Jaume Puy [a], Claudia A. Blindauer [b], Josep Galceran [a,*]

[a] Departament de Química, Universitat de Lleida, and AGROTECNIO-CERCA, Rovira Roure 191, 25198, Lleida, Catalonia, Spain
[b] Department of Chemistry, University of Warwick, Coventry, CV4 7AL, UK

HIGHLIGHTS

- Free Zn concentration, $[Zn^{2+}]$, in biological samples can be determined with the AGNES technique.
- $[Zn^{2+}] = 2.7 \pm 0.2$ nmol L^{-1} was found at pH = 7.0, total Zn 20 μmol L^{-1} and Bovine Serum Albumin 600 μmol L^{-1}
- A sample of Fetal Bovine Serum yielded $[Zn^{2+}] = 0.25 \pm 0.02$ nmol L^{-1}

GRAPHICAL ABSTRACT

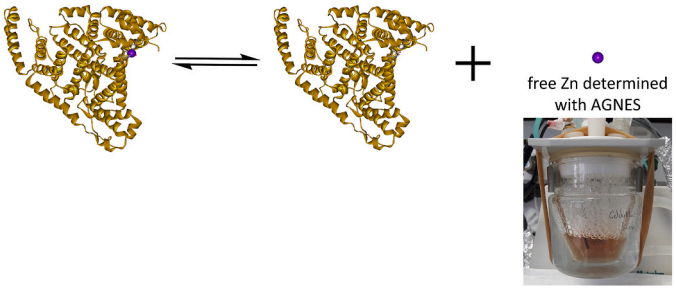

ARTICLE INFO

Keywords:
Speciation
Electrodic adsorption
Bovine serum albumin
Fetal bovine serum

ABSTRACT

The speciation of essential metal ions in biological fluids, such as blood plasma and serum, is of fundamental importance to understand the homeostasis of these elements. The activity of metal ions such as Zn^{2+} in extracellular media is thought to affect their interaction with membrane-bound transporters, and thus is critical for their cellular uptake. Previous approaches to determine "free" Zn^{2+} (i.e. the hexa-aquo ion) are based on separation by either chromatography or ultrafiltration, or on metallochromic dyes. However, both types of approach are prone to affect the relevant equilibria. These drawbacks can be circumvented with the electroanalytical technique AGNES (Absence of Gradients and Nernstian Equilibrium Stripping), since it can measure free zinc concentration without perturbing the sample speciation. Here, a Bovine Serum Albumin (BSA) + Zn synthetic mixture and Fetal Bovine Serum (FBS) are analyzed as proof of concept. Adsorption of BSA on the surface of the Hanging Mercury Drop Electrode (HMDE), despite the advantage of its renewal, is so intense that it blocks appropriate attainment of the required equilibrium, and only estimations of $[Zn^{2+}]$ can be derived. In contrast, a rotating disc electrode with a thin mercury film deposited on it (TMF-RDE) is advantageous because of its small volume and enhanced mass transfer. Protein adsorption can be prevented by covering the TMF-RDE with Nafion. A free Zn concentration $[Zn^{2+}] = 2.7$ nmol L^{-1} was found at pH 7.0, total Zn 20 μmol L^{-1} and BSA 600 μmol L^{-1}. A sample of FBS with fixed pH 7.2 (MOPS 0.08 mol L^{-1}) yielded $[Zn^{2+}] = 0.25$ nmol L^{-1}. This methodology opens the way to free metal concentration determinations in biological fluids.

* Corresponding author.
E-mail address: galceran@quimica.udl.cat (J. Galceran).

https://doi.org/10.1016/j.aca.2022.340195
Received 4 May 2022; Received in revised form 25 June 2022; Accepted 19 July 2022
Available online 31 July 2022

1. Introduction

Metal ions have critical roles in biological systems, illustrated by the fact that about half of all enzymes require at least one metal ion to function [1]. Amongst essential metals, zinc is perhaps the most versatile, with about 10% of the human proteome estimated to correspond to zinc-requiring proteins [2]. This pervasiveness is also reflected in the manifold biological processes that require the involvement of zinc [3], which include regulation of gene expression and cell cycle progression [4], energy metabolism [5], the immune system [6], host-pathogen interactions [7], hemostasis [8] and neurochemical processes involved in learning and memory [9]. Correspondingly, zinc deficiency or disturbances in zinc metabolism promote a range of disorders, including impairment of cognitive and immune functions, growth retardation, and diabetes [10]. For many of these processes and disorders, it is clear that understanding zinc dynamics in space and time is critical. Recent years have therefore seen a reinforced interest in zinc homeostasis in general [11,12], and in zinc signalling [13–16] and "mobile" zinc in particular [4,14,17].

Central to understanding the actions of zinc in biological systems is a quantitative description of its speciation, namely how much of the total Zn^{2+} is bound to ligands such as proteins and small molecules, and how much is "free". This issue is more complicated than might be expected. Typically, biological solutions are highly complex and contain an excess of sites/ligands with metal-binding ability. In consequence, a variety of terms including "free", "labile", "mobile", "exchangeable" and "available" are used to describe the proportion of Zn^{2+} of interest in the context of transport and signalling. The issue is further confounded by the fact that it is often not clear [18,19] what is measured with the most commonly used approach to address mobile Zn^{2+}, namely the utilization of zinc-responsive fluorescent dyes. Fluorescent zinc sensors are undoubtedly powerful tools to detect "mobile" or "available" zinc, and also allow monitoring changes in a range of zinc pools in real time [20–23]. However, questions have been raised regarding what the observed analytical signal corresponds to in terms of absolute quantitation [21]. It has been demonstrated that besides interacting with non-protein-bound Zn^{2+}, many fluorescent zinc sensors also form ternary complexes with protein-bound Zn^{2+} [24–26]. In addition, formation of ternary complexes with small molecules present in biological solutions also may confound quantitation [19,27,28]. It is therefore clear that it would be highly desirable to have complementary methodologies available to measure and benchmark the quantitative determination of a physico-chemically well-defined species, ideally the free Zn^{2+} hexaquo ion. Indeed, the concentration of such "free" Zn^{2+} is thought to determine zinc uptake into cells [29], and free serum or plasma Zn^{2+} has been proposed to be a better marker of zinc status than total zinc [30].

In the present work, we choose for our proof-of-concept study Fetal Bovine Serum (FBS), a complex extracellular medium that finds widespread application in cell biology. It is a little-appreciated fact that amongst other nutrients, FBS also supplies both zinc and at least one zinc-buffering molecule, namely serum albumin [31]. Its composition is also closely related to that of human serum, which is of course of biomedical interest (*vide infra*). Although the subject of a few early studies [32–34], zinc speciation in the extracellular space has received comparatively little recent attention [30,35,36], despite the fact that there is clear evidence that extracellular zinc speciation has profound effects, for example on immune cells [29]. It is also critically important to appreciate that free Zn^{2+} in the extracellular space is cytotoxic at concentrations as low as nanomolar [37]. Such effects are likely mediated by cellular zinc uptake depending on availability of free Zn^{2+}. Indeed, at least some membrane-bound zinc uptake transporters are known to function in an electrodiffusional manner, with transport directly dependent on the gradient in free Zn^{2+} [38]. Thus, although *in vivo* only 0.1% of body zinc resides in blood plasma [39], it turns over about 150 times a day [3] and its total levels and speciation govern not only zinc-dependent processes in this compartment (including hemostasis [40], insulin activity [5], and response to pathogens [41]), but ultimately also affect transfer from plasma to all organs and tissues, and hence whole-body zinc homeostasis [3]. Studying zinc speciation in serum and plasma is therefore a matter of central importance [30].

In conclusion, there is a need for developing analytical techniques able to determine the free concentration, $[Zn^{2+}]$, in biological samples. This challenge is tackled here by extending the electroanalytical technique AGNES (Absence of Gradients and Nernstian Equilibrium Stripping) [42], which has successfully measured $[Zn^{2+}]$ in a variety of systems [43]: i) inorganic ligand titrations; ii) humic acids titrations [44,45]; iii) red and white wine [46,47]; iv) dispersions of ZnO nanoparticles [48,49]; v) river, estuarine and seawater [50,51]; vi) soil extracts [52]; and more. Specific difficulties arising in biological systems are the low levels of free concentrations and the complexity of the matrix, with a large variety of compounds prone to adsorb onto the electrode surface. As shown here, these difficulties can be overcome with the use of the Thin Mercury Film Rotating Disc Electrode (with a very favourable surface-to-volume ratio and enhanced mass transport) and with the covering of the electrode with a Nafion layer (that protects from adsorption). The layout of the article is as follows. In section 2 special practical issues (such as the preparation of the Nafion-covered Thin Mercury Film Rotating Disc Electrode) are emphasized. In section 3, the limitations of typical non-covered electrodes (where adsorption might occur) are shown, together with the satisfactory measurements of $[Zn^{2+}]$ in a synthetic mixture with Bovine Serum Albumin (BSA) or directly in a buffered sample of Fetal Bovine Serum (FBS). Section 4 discusses the consistency of the new results with published literature, while section 5 presents the main conclusions.

2. Experimental section

2.1. Reagents

All solutions were prepared with ultrapure water (18.2 MΩ cm, Synergy UV purification System Millipore). Zn^{2+} and Hg^{2+} solutions were prepared from 1000 mg L^{-1} standards (Merck, Certipur®). Ionic strength was adjusted with KNO_3 (Merck, 99.995% Suprapur®). MOPS (3-(N-morpholino)-propanesulfonic acid, Sigma-Aldrich, BioXtra ≥99.5%) was used as pH-buffer. pH was adjusted with 0.1 mol L^{-1} HNO_3 or 1 mol L^{-1} KOH (both from Merck, Titripur®). The solution for the coating of the glassy carbon rotating disc was prepared by dissolving Nafion® 117 at 5% (Lot BCCC5483, Sigma-Aldrich) in an ethanol-water (90:10 v/v) mixture so that the ratio was 0.4%. Bovine serum albumin (BSA, lyophilized powder, 98%) was from Sigma-Aldrich. Fetal bovine serum (FBS, lot BCBW3466, heat inactivated, non-USA origin) was from Sigma-Aldrich. NH_4Ac, NH_4SCN (both from Merck, Emsure®) and 0.5 mol L^{-1} HCl (FisherScientific, Trace Metal Grade) were used to prepare the cleaning solution of the rotating electrode and the reoxidation of the mercury film.

The BSA + Zn solution was prepared by adding, to 25 mL of 0.15 mol L^{-1} KNO_3, the necessary amounts of solid to reach 600 μμmol L^{-1} in BSA and 0.045 mol L^{-1} in MOPS. The solution was continuously stirred until complete dissolution, and then $Zn(NO_3)_2$ was added from a stock of 100 mg L^{-1}, prepared from 1000 mg L^{-1} standard solution (in 2% HNO_3, Merck, Certipur®), to a final concentration of 20 μμmol L^{-1} in Zn^{2+}, followed by adjustment of pH to 7.0 with 1 mol L^{-1} KOH. N_2 (purity≥ 99.999%) was bubbled for 3 min, then the flask was closed and kept at 25 °C for the next day.

FBS was received frozen and kept at −20 °C. Frozen samples of 500 mL were thawed at room temperature and divided into 25 mL aliquots and were re-frozen until they were used.

Once a sample for measurement was thawed, pH was measured. MOPS was added to a final concentration of 0.08 mol L^{-1}, and pH was adjusted to 7.2 (close to the initial pH value) with 1 mol L^{-1} KOH. N_2 was bubbled for 3 min, then the flask was closed and kept at 25 °C for the next day. To ensure that pH was stable, it was checked again just before

starting AGNES experiments.

The total Zn content in FBS was quantified by Inductively Coupled Plasma Mass Spectrometry using a dilution matrix, composed of 2% (w/v) 1-butanol (Merck, ACS Reagent, 99,4%), 0.05% (w/v) EDTA (ACROS 99% Pure), the non-ionic surfactant Triton X-100 0.05% (w/v) (Sigma, BioXtra) and 1% (w/v) NH_4OH (Sigma-Aldrich, ACS Reagent).

2.2. Apparatus

Voltammetric measurements were carried out with Autolab PGSTAT101 or with μAutolab Type III potentiostats attached to a Metrohm 663 VA stand, controlled with GPES 4.9 (EcoChemie) or NOVA 1.11 (Metrohm Autolab) softwares. All measurements were performed in a conventional three electrode glass cell. The working electrode was either a Metrohm Hanging Mercury Drop Electrode (drop size 1 for AGNES and size 3 for Differential Pulse Polarography) or a glassy carbon rotating disc electrode (2 mm diameter, Metrohm) plated with a thin mercury film (see next section). Glassy carbon was used in the auxiliary electrode and the reference electrode was double-junction Ag/AgCl/3 mol L^{-1-1} KCl with 0.1 mol L^{-1-1} KNO_3 in the salt bridge. A glass jacketed cell was used in all the experiments and thermostated at 25 °C. A glass combined electrode (Hach 5209) was attached to an Orion Dual Star ion analyzer (Thermo) and introduced into the cell to monitor the pH. During the measurements with AGNES, the glass electrode was disconnected to avoid possible interferences. Solutions were thoroughly deaerated with N_2 to minimize the presence of oxygen (which is also reduced at the electrode surface and, when in high levels, interferes with accurate quantification).

An Advantage Lab Sonicator, AL 04-03 was used for the preparation of the TMF-RDE electrode.

Total zinc was quantified using a 7700x ICP-MS (Agilent Technologies, Inc, Tokyo, Japan) with Ni sampler and skimmer cons, a MicroMist glass concentric nebulizer and a He collision cell. The operating conditions were as follows: RF power 1550 W, carrier gas flow rate 1.01 L min^{-1}, helium collision gas flow rate, 4.3 mL min^{-1}, spray chamber temperature 2.0 °C, sample depth 10.0 mm, nebulizer pump 0.1 rps, extract lens 1 voltage 0.0 V and extract lens 2 voltage −1.95.0 V. The monitored isotope was ^{66}Zn and on-line internal standard ^{72}Ge. Appropriate amounts of standard stock solutions containing 1000 mg L^{-1} in 2% nitric acid of Zn^{2+} (High Purity Standard) were mixed with the dilution matrix to prepare standard solutions and then used to construct the calibration curve. For the FBS sample, a dilution factor of 20 was used (125 μL of sample in 2.5 mL of dilution matrix). 3 replicates of the FBS sample were analysed.

2.3. Nafion-coated TMF-RDE electrode

The Nafion-coated Thin-Mercury-Film Rotating-Disc-Electrode was prepared daily, essentially following the protocol developed by Vidal et al. [53].The steps were:

1. Polish the glassy carbon disc with alumina 0.3 μm (Metrohm) for 1 min.
2. Clean with ethanol, followed by water.
3. Sonicate in water for 2 min.
4. Run an electrochemical pre-treatment of 50 successive cyclic voltammograms between −0.8 V and +0.8 V at 0.1 V s^{-1} in a 1.0 mol L^{-1} NH_4Ac/0.5 mol L^{-1} HCl solution [54,55].
5. Clean thoroughly with water and dry with sorbent paper.
6. Take the electrode out of the cell and place it in a support, so that the disc surface is horizontal and looking upward and, then, add to the disc 10 μL of 0.4% Nafion solution. Spread the added solution gently all over the disc surface by manually rotating the electrode with a slight tilt. Three different concentrations of Nafion® have been evaluated here: 0.4%, 1% and 5%. The one at 0.4% was finally chosen because of its better performance in terms of less oxygen current and shorter required deposition times (data not shown).
7. Evaporate the solvent for 20 min at room temperature.
8. Cure with a hair-drier at approximately 50 °C for 2 min.
9. Return the electrode to the voltammetric cell and plate the mercury film: a) immerse the electrode in a solution 0.24 mmol L^{-1} $Hg(NO_3)_2$ and 0.15 mol L^{-1} HNO_3 (adjusted to pH 1.9); b) purge with N_2 for 300 s and c) deposit at −1.3 V for 420 s while rotating at 1000 rpm [55].
10. Once AGNES experiments are finished, the charge associated to the deposited Hg can be quantified with a linear sweep ν = 0.005 V s^{-1} from −0.15 V to +0.4 V in a solution 1 mol L^{-1} NH_4SCN (pH = 4.5). We sweep as many times as necessary (usually twice) until the new reoxidation load in one sweep associated with the Hg is zero, thereby ensuring that we remove all the Hg initially deposited. The daily reoxidation value helps us to obtain the volume of mercury deposited each time that we prepare the electrode and, thus, ensure that we have a reproducible electrode volume.

2.4. AGNES technique

AGNES is a stripping technique where the analyte, accumulated in the amalgam during the first (or deposition) stage, is quantified in the second (or stripping) stage.

2.4.1. First stage

The distinctive characteristic of AGNES is that the deposition has to last until the fulfilment of a special equilibrium situation where there are no gradients in the concentrations profiles (neither in the solution, nor in the amalgam) and Nernstian equilibrium holds at the electrode surface [56]. The ratio between concentrations at either side of the electrode surface is the gain or preconcentration factor Y, which – due to Nernst's law – can be computed as:

$$Y = \frac{[Zn^0]}{[Zn^{2+}]} = \exp\left[-\frac{2F}{RT}\left(E_1 - E^{0'}\right)\right]. \quad (1)$$

where F is the Faraday constant, R the gas constant, T the temperature, $E^{0'}$ the formal standard redox potential and E_1 is the deposition potential. By changing E_1, one prescribes different gains, thus changing the limit of detection and the required deposition time. Nernst's law relates activities of the ion in solution and in the reduced form, and accordingly, the gain (in concentrations) is ionic strength dependent. When calibration and measurement are not run at a common ionic strength, a simple correction using the activity coefficients can be applied (see eqn. (2) in Ref. [56]).

To avoid an explicit calculation of $E^{0'}$, the gains are computed here from an ancillary Differential Pulse Polarography (DPP) experiment performed with a large drop in the HMDE (so that the simple expression for planar diffusion applies). Then,

$$Y = \sqrt{\frac{D_{Zn^{2+}}}{D_{Zn^0}}}\exp\left[-\frac{nF}{RT}\left(E_1 - E_{peak} - \frac{\Delta E}{2}\right)\right] \quad (2)$$

where E_{peak} is the DPP peak potential and ΔE is the modulation amplitude of the DPP experiment. If a laboratory without HMDE wanted to implement AGNES, they could obtain the gain from a calibration and an estimation of the electrode volume [57] or from any other technique providing $E^{0'}$.

To achieve equilibrium, two variants of AGNES for the deposition stage can be used:

- AGNES-1P, where the same deposition potential E_1 is applied along the first stage (during t_1 seconds). The eventual stabilization of

trajectories (i.e. time-course experiments with a fixed gain) in a plateau for sufficiently long deposition times indicates the fulfilment of AGNES requirements.

- AGNES-2P, where the first stage is split in two [58]. During the first sub-stage ($t_{1,a}$ seconds) a very negative potential is applied, so that it drives a large flux of the analyte towards the electrode. During a second sub-stage ($t_{1,b}$ seconds), the deposition potential E_1 (corresponding to the aimed gain Y) is applied. If $t_{1,a}$ is adequate, at the beginning of the second sub-stage there will practically already be the prescribed amount of reduced metal in the amalgam, so that relatively short $t_{1,b}$ will be enough to reach equilibrium. If $t_{1,a}$ is too long, there will be an excess of reduced metal accumulated in the electrode for short $t_{1,b}$ times (i.e. an "overshoot"). If $t_{1,a}$ is too short, the amount of reduced metal accumulated in the electrode will be less than the amount desired, so this is described as "undershoot". Again, AGNES equilibrium is recognised in the eventual plateau for sufficiently long $t_{1,b}$ times. AGNES-2P can reduce the required deposition times up to a factor of 10 with respect to AGNES-1P.

2.4.2. Second stage

The amount of accumulated analyte can be quantified in the second stage *via* the current or the charge, leading to several variants. When using the RDE, we have applied AGNES-SCP [59], where a fixed stripping current I_s is prescribed and the recording of the potential evolution yields a transition time τ, from which the charge can be computed as

$$Q = (I_s - I_{Ox})\tau. \quad (3)$$

where I_{Ox} is the current due to oxidant species (measured along the waiting time at the end of the first stage, while E_1 is being applied without any stirring).

2.4.3. Fundamental AGNES relationship

By combining Nernst's and Faraday's laws, the fundamental equation of AGNES can be established:

$$Q = Y\ \eta_Q\ \left[Zn^{2+}\right]. \quad (4)$$

where η_Q is a proportionality factor that has been found from a calibration experiment, where Q (for stabilized responses, i.e. equilibrium values) is plotted *versus* $[Zn^{2+}]$. This calibration is performed on a synthetic solution with background electrolyte KNO_3 (at the same ionic strength as the sample to be analyzed) and increasing amounts of added total Zn, where $[Zn^{2+}]$ is computed with the speciation program Visual MINTEQ. For simplicity reasons (no adsorption on the walls, simpler speciation, etc.), calibrations were performed here at pH 5.5. Representative examples of calibrations are given in the Supporting Information.

In conclusion, free Zn concentration can be found from eqn (4) and from the reading of the stripped charge Q (computed with eqn (3)).

2.4.4. Specifics of BSA and FBS systems

The studied systems exhibited a high viscosity and a pronounced tendency to foam when the solutions were purged with N_2 or even when the RDE was spinning and producing an associated stirring. We noticed that if the cell overhead was full of foam, I_{Ox} could surpass the value of I_s and the term in brackets in eqn. (3) became so large that the transition time was too small to be accurately determined or even seen. To achieve a better control over the N_2 flux, a rotameter was installed. We found that 2 h purging at 4 L h^{-1} before the start of AGNES experiments was enough to reduce I_{Ox} to suitable levels. To avoid the contact between the foam and the metallic head of the RDE shaft, this was protected with Teflon film and 3 min were left in between measurements to allow for some collapse of the foam on top of the analyzed solution.

3. Results

3.1. HMDE exploration of BSA + Zn system

As an example for a simple, but well-defined synthetic biological system, we worked with BSA (600 μmol L^{-1}, a concentration close to that present in plasma/serum [60]) in 0.15 mol L^{-1} KNO_3, 0.045 mol L^{-1} MOPS buffer at pH 7.0, mixed with a total Zn^{2+} concentration $c_{T,Zn} = 20$ μmol L^{-1}. The latter concentration was chosen to match typical plasma/serum total zinc concentrations [61]. Based on reported stability constants [62,63], we initially estimated a $[Zn^{2+}]$ between 1 and 100 nmol L^{-1}. For the HMDE, we have applied (for the second stage) the variant AGNES-I, where the stripping potential is sufficiently less negative as to force diffusion-limited conditions for the re-oxidation of Zn°. In these conditions, the faradic intensity current is proportional to the gain and to $[Zn^{2+}]$, in an equation parallel to (4) with a normalized proportionality factor (η) from a suitable calibration. With the two-pulse strategy in the first stage, we could estimate $[Zn^{2+}] \approx 4.48$ nmol L^{-1}, by averaging values for $t_{1,b}$ from 2000 s to 4000 s (see Fig. 1). The obtained value is not accurate, because the different trajectories (i.e. time-course series) with a common gain, but different $t_{1,a}$, did not completely converge (as it would be desired to fulfil AGNES conditions), despite the very long $t_{1,b}$ endured. Indeed, short $t_{1,b}$ times allow to diagnose an overshoot for $t_{1,a} = 150$ s, but this overshoot does not relax towards a common equilibrium value at longer times (i.e. the series does not merge with series with shorter $t_{1,a}$). This kind of "anomalous" behaviour, with increasing $t_{1,b}$ not being able to relax towards equilibrium, has already been seen in complex matrices, such as wine [46] or ZnO nanoparticles with a dispersant [56], and can be interpreted as being due to the adsorption of organic molecules onto the mercury electrode (either blocking the passage or rendering the electrodic charge transfer irreversible). The advantage provided by the renewal of the drops in HMDE is not sufficient to overcome the extreme adsorption impact in this case, because the low concentration in the sample requires high gains and, thus, long deposition times.

3.2. TMF-RDE without protection

The rotating disc, with a larger surface-to-volume ratio and an enhanced mass transport [54,55,64], can give access to larger gains for a fixed time, or require shorter times for a fixed gain. Trials with the standard TMF-RDE ("bare" in the sense of not having a layer to prevent the direct contact of the solution with the mercury electrode, which is prepared following the methodology of section 2.3 but omitting steps 6, 7 and 8) in the same synthetic system (0.15 mol L^{-1} KNO_3 + 0.045 mol L^{-1} MOPS + 600 μμmol L^{-1} BSA + $c_{T,Zn}$ = 20 μμmol L^{-1} at pH 7.0) resulted in an anomalous behaviour with decreasing charges for longer deposition times when using AGNES-1P, with $Y = 5 \times \times 10^5$. Again, this was interpreted as due to extremely strong electrodic adsorption. Therefore, we explored next whether this could be prevented by coating with Nafion.

3.3. Nafion protected TMF-RDE

A protective ion exchange film can be interposed between the mercury electrode and the solution, and, thus, avoid electrodic adsorption by size exclusion and/or by electrostatic repulsion [65]. This strategy has been used in various contexts [53,66–70]. For instance, ascorbate anion was reported [71] to be excluded from a Nafion coating when determining dopamine.

Following the work of Vidal et al. [53], here the Nafion film is laid before the mercury deposition, as described in the Materials and Methods section, since mercury ions can permeate the already existing Nafion film and reach the glassy carbon surface and generate Hg nanodroplets there.

To assess whether the coverage with Nafion introduces some time

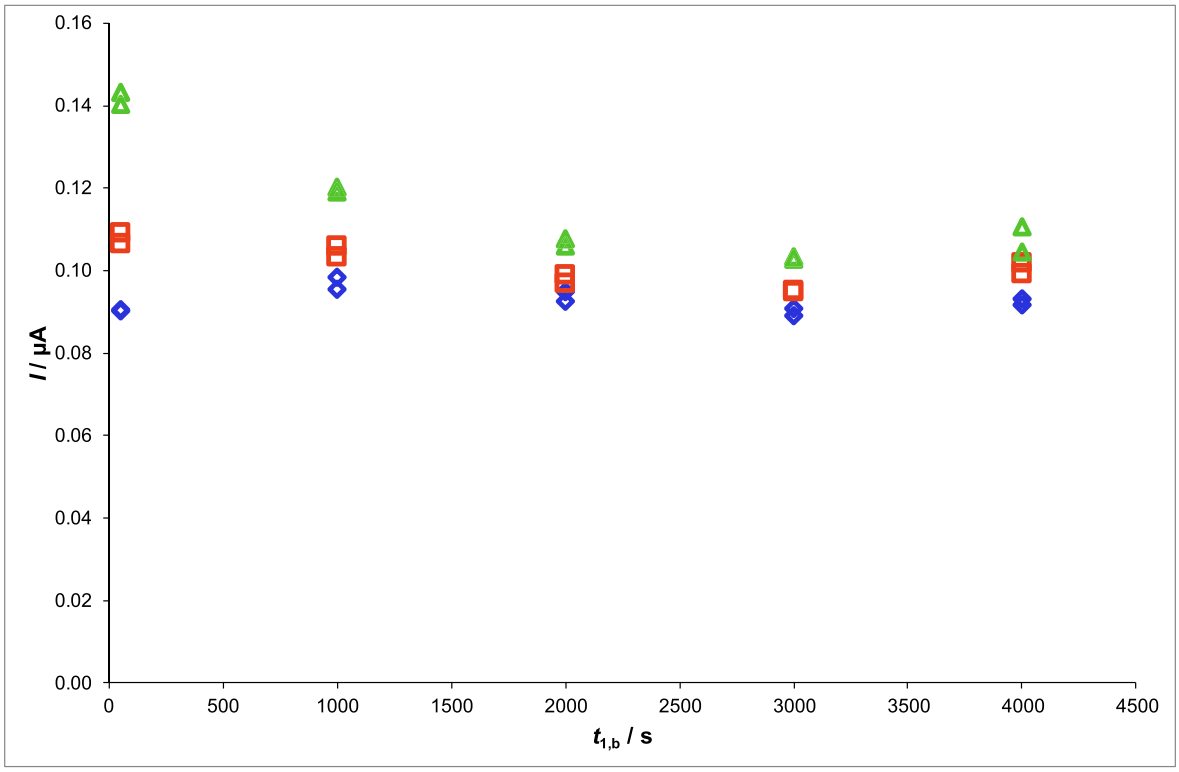

Fig. 1. Lack of full convergence of AGNES-2P trajectories when using the Hanging Mercury Drop Electrode. Markers: blue diamonds for $t_{1,a} = 75$ s; red square for $t_{1,a} = 100$ s and green triangle for $t_{1,a} = 150$ s, all of them with $Y = 1 \times \times 10^4$. Gain of the first substage in all experiments $Y_{1,a} = 5 \times \times 10^8$. Composition of sample: 0.15 mol L^{-1} KNO_3 + 0.045 mol L^{-1} MOPS +600 µmol L^{-1} BSA + $c_{T,Zn} = 20$ µmol L^{-1} at pH 7. (For interpretation of the references to colour in this figure legend, the reader is referred to the Web version of this article.)

delay in the achievement of equilibrium, AGNES-1P trajectories at various gains were conducted in a solution without any relevant ligand (i.e. no BSA), see Fig. 2A. When replotted in normalized charges and times, see Fig. 2B, the collapse of all trajectories confirms the achievement of Nernstian equilibrium in each of their plateaus. From the figure, one derives the following rule of time:

$$t_1 - t_w = 0.006 \times Y \quad (5)$$

which is practically identical to the one reported for Zn in the TMF-RDE without coverage [51], indicating a negligible impact (in deposition efficiency) from the addition of the Nafion coating.

Given the polyelectrolytic nature of the Nafion film [65,72], some enrichment (partition) of Zn^{2+} is expected in it (with respect to the bulk concentration in the sample solution) depending on the ionic strength (essentially due to the principal ions in the solution). In the ensuing Donnan equilibrium, a cation with charge n + will be enriched by a factor χ^n where χ is the so-called Boltzmann factor [47]. So, instead of one equilibrium between Zn^{2+} in the sample and Zn° in the amalgam, we now have two coupled equilibria: A) between Zn^{2+} in the sample and Zn^{2+} in the Nafion layer (with $[Zn^{2+}]_{Nafion} = \chi^2\ [Zn^{2+}]$) and B) between Zn^{2+} in the Nafion layer and Zn° in the amalgam.

The presence of the interposed Nafion coating, with two successive equilibria, does not alter the equilibrium relationship Y between [Zn°] and $[Zn^{2+}]$, because Y only depends on the potential E_1 (between the reference electrode, which is in direct contact with the sample solution, and the working electrode where Zn° has been accumulated) as prescribed by eqn. (1)

In order to avoid the exchange of ions between the solution and the Nafion film (which delayed the stabilization of AGNES signal in control experiments with fixed conditions), the plating solution was also set to the ionic strength of the experiment (i.e. solutions were fixed at a similar enough ionic strength).

3.3.1. $[Zn^{2+}]$ in the synthetic BSA system from Nafion TMF-RDE measurements

AGNES-2P was applied to the synthetic solution (0.15 mol L^{-1} KNO_3, 0.045 mol L^{-1} MOPS, 600 µmol L^{-1} BSA and $c_{T,Zn} = 20$ µmol L^{-1}, pH 7.0) with the Nafion-covered RDE. As we had seen very sluggish relaxation towards equilibrium in the case of HMDE, we looked for a combination of parameters where the convergence towards equilibrium could be clearly revealed (with merging overshoots and undershoots), and so, unambiguously ascertain the fulfilment of AGNES conditions (see Fig. 3). The combinations ($Y = 2 \times \times 10^6$, $t_{1,a} = 60$ s, blue diamonds) and ($Y = 5 \times \times 10^6$, $t_{1,a} = 275$ s, green triangles) are clear undershoots, where the amount of Zn° accumulated at the end of the first sub-stage is below the one required at equilibrium. For instance, the undershoot is seen in Fig. 3 as the value of the charge for the point ($Y = 2 \times \times 10^6$, $t_{1,a} = 60$ s, $t_{1,b} = 50$ s) is less than that for the point ($Y = 2 \times \times 10^6$, $t_{1,a} = 60$ s, $t_{1,b} = 400$ s). The combinations ($Y = 2 \times \times 10^6$, $t_{1,a} = 160$ s, pink squares) and ($Y = 5 \times \times 10^6$, $t_{1,a} = 400$ s, purple circles) are overshoots. There is a merging of one undershoot and one overshoot for each gain, confirming the attainment of equilibrium at the largest $t_{1,b}$. Moreover, the retrieved equilibrium charges at both gains are in the Nernstian proportion of the gains (1:2.5), as required. The merging of overshoot and undershoot trajectories together with their plateau charges fulfilling a Nernst relationship unequivocally corroborate the attainment of AGNES conditions. With this kind of experiments in three different solutions, we determined $[Zn^{2+}] = 2.7 \pm 0.2$ nmol L^{-1} (see Fig. 3 and Table 1).

3.3.2. $[Zn^{2+}]$ in MOPS-buffered FBS from Nafion TMF-RDE measurements

The total zinc concentration in FBS was determined by ICP-MS as $c_{T,Zn} = 45.2 \pm 0.3$ µµmol L^{-1}. Preliminary results (not shown) on the determination of $[Zn^{2+}]$ with AGNES in FBS without any buffer indicated that the pH of the FBS increased by up to one pH unit during the

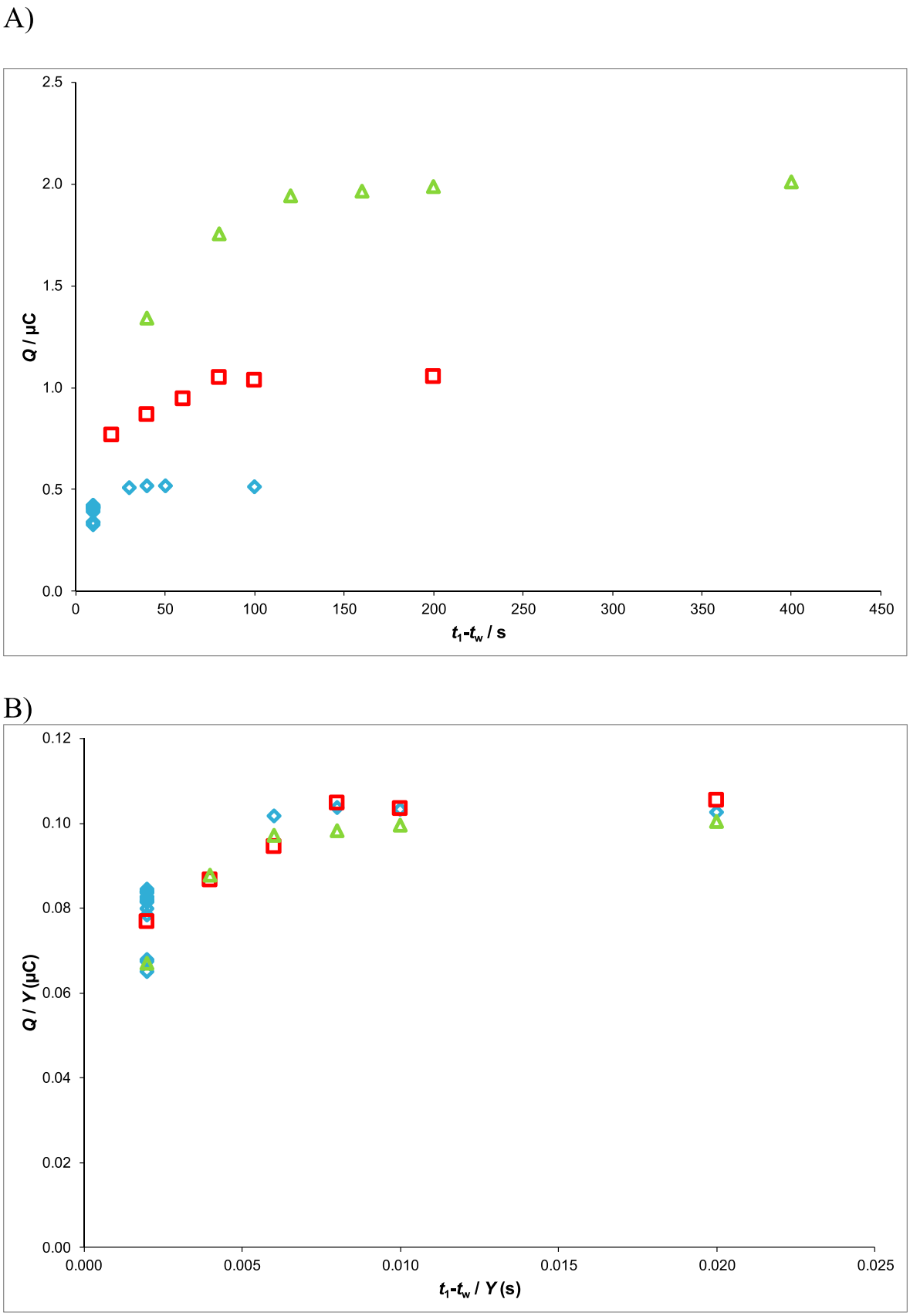

Fig. 2. Collapse of AGNES-1P trajectories with the Nafion-covered TMF-RDE leading to the time rule given in eqn. (5). A) charge trajectories; b) normalized representation. Markers: blue diamonds for $Y = 5 \times \times 10^{3}$; red square for $Y = 1 \times \times 10^{4}$ and green triangle for $Y = 2 \times \times 10^{4}$. Composition of solution: 0.15 mol L^{-1} KNO_3 + $c_{T,Zn} = 1 \times \times 10^{-6}$ mol L^{-1} at pH = 5.5. (For interpretation of the references to colour in this figure legend, the reader is referred to the Web version of this article.)

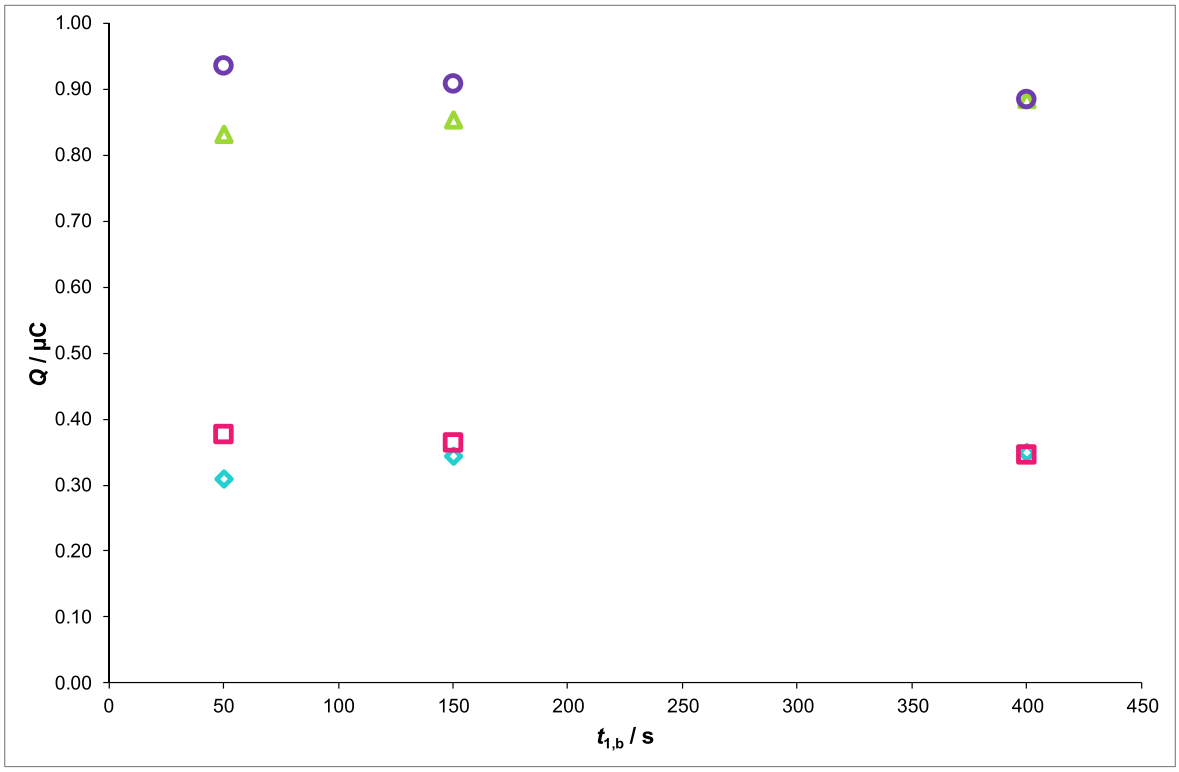

Fig. 3. Convergence of the charge trajectories (obtained using the Nafion-covered TMF-RDE) towards equilibrium values that are also in the Nernstian proportion among them. Markers: blue diamond for $t_{1,a} = 60$ s with $Y = 2 \times \times 10^6$; pink square for $t_{1,a} = 160$ s with $Y = 2 \times \times 10^6$; green triangle for $t_{1,a} = 275$ s with $Y = 5 \times \times 10^6$ and purple circle for $t_{1,a} = 400$ s with $Y = 5 \times \times 10^6$. Gain of the first sub-stage in all experiments $Y_{1,a} = 5 \times \times 10^8$. Composition of sample: 0.15 mol L^{-1} KNO_3 + 0.045 mol L^{-1} MOPS +600 µmol L^{-1} BSA + $c_{T,Zn} = 20$ µmol L^{-1} at pH 7.0. (For interpretation of the references to colour in this figure legend, the reader is referred to the Web version of this article.)

Table 1
Compilation of $[Zn^{2+}]$ determined by AGNES in a mixture of 600 µmol L^{-1} BSA, $c_{T,Zn} = 20$ µmol L^{-1}, 0.15 M KNO_3, 0.045 mol L^{-1} MOPS, pH = 7.0 at 25 °C with the Nafion® TMF-RDE. In all cases $t_{1,b} = 400$ s.

Replicate	Y	$t_{1,a}$/ s	τ/ms	Q/µC	η_Q/mC mol^{-1} L	$[Zn^{2+}]$/nmol L^{-1}
1	$2 \times \times 10^6$	60	112	0.349	0.0693	2.52
		160	110			2.50
	$5 \times \times 10^6$	275	278	0.885	0.0693	2.55
		400	273			2.55
2	$2 \times \times 10^6$	60	130	0.392	0.0693	2.83
		160	124			2.83
	$5 \times \times 10^6$	275	306	0.979	0.0693	2.82
		400	301			2.83
					average	**2.7**
					σ	**0.2**

day, most likely due to the removal of CO_2 during successive N_2 purges. Therefore, we performed the subsequent experiments with the addition of MOPS buffer (0.08 mol L^{-1}) prior to purging, and re-adjustment of the pH to 7.2 after purging. Assuming for FBS an initial ionic strength as that for serum [73], the addition of MOPS raises it to 0.154 mol L^{-1}, which is sufficiently close to that of the calibration (KNO_3 0.15 mol L^{-1}), so that essentially no correction for ionic strength is needed. Fig. 4 shows an example of one replicate where the series at the lowest gain ($Y = 5 \times \times 10^6$, see purple diamonds) exhibited an undershoot for $t_{1,a} = 30$ s and $t_{1,b}$ shorter than 200 s, but reached an essential constant plateau for $t_{1,b}$ of 200 and 400 s. By doubling the gain and $t_{1,a}$ (see series with red triangles in Fig. 4), the plateau was reached for $t_{1,b}$ of 200 and 400 s, at a charge double of that obtained for the lowest gain, as prescribed by Nernst's law. The two plateau values of the charge led to two values of $[Zn^{2+}]$ for this replicate. Table 2 gathers this and the results from two other replicates (acquired for different aliquots at different days) and shows that the determined average free zinc concentration in the sample was $[Zn^{2+}] = 0.25 \pm 0.02$ nmol L^{-1}. This represents a very low fraction of 0.55% of total Zn being free in these samples.

4. Discussion

In this study, the free Zn concentration, $[Zn^{2+}]$, in a synthetic solution containing a high protein (BSA) concentration and in a natural system (FBS) has been directly and robustly measured with AGNES (variant 2P for the first stage, variant SCP for the second stage). A key advancement is provided by the use of the TMF-RDE covered with a Nafion coating which effectively avoids extreme electrodic adsorption. On the one hand, the deposition times are relatively short and close to those for the bare electrode, despite the interposed coating. This is probably due to its thinness. On the other hand, the existing electrostatic enrichment in the Nafion coating does not impact on the effective gain applied, because just one added equilibrated phase is bridging the resulting equilibrium between the concentrations of Zn° in the amalgam and of Zn^{2+} in the bulk solution. One caveat is the possibility of some denaturation of the proteins due to stirring, although the extent might be negligible (1.8% reported in human serum albumin monomers, [74]) and with a reversible character [75].

The free Zn concentration found in this work in the BSA mixture (2.7 mol L^{-1}) is consistent with estimates based on published stability constants. The logarithm of the stoichiometric, pH-independent stability constants (also known as "intrinsic constants" [76]) determined for Zn-BSA range from 7.0 to 7.6 [76–78] (at $I \approx 0.1$ mol L^{-1}). Together with a $pK_a = 8.2$ for the major binding site (determined by studying the pH dependence of zinc binding to BSA [76]), this yields conditional stability constants ranging from log K' = 5.77 to 6.37 at pH 7.0. From these, $[Zn^{2+}]$ can be estimated to range from 14.7 to -58.4 nmol L^{-1}.

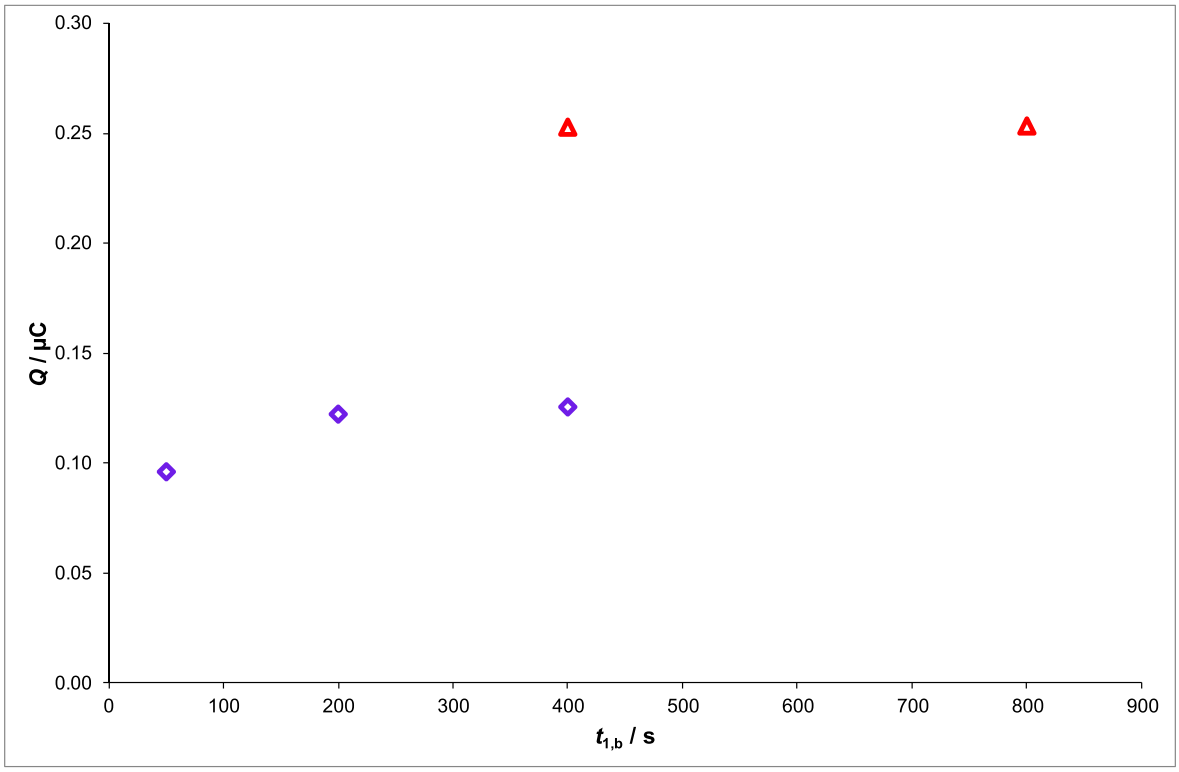

Fig. 4. Simple trajectories towards equilibrium values that are also in the Nernstian proportion when using the Nafion-covered TMF-RDE in Fetal Bovine Serum +0.08 mol L^{-1}MOPS, pH 7.2. Markers: purple diamond for $t_{1,a} = 30$ s with $Y = 5 \times \times 10^6$; red triangle for $t_{1,a} = 60$ s with $Y = 1 \times \times 10^7$. Gain of the first sub-stage in all experiments $Y_{1,a} = 5 \times \times 10^8$. (For interpretation of the references to colour in this figure legend, the reader is referred to the Web version of this article.)

Table 2
Compilation of $[Zn^{2+}]$ determined by AGNES in samples of FBS (lot BCBW3466) + 0.08 mol L^{-1} MOPS with the Nafion® TMF-RDE. pH = 7.2 at 25 °C. In all cases $t_{1,b} = 400$ s.

Replicate	Y	$t_{1,a}$/ s	τ/ms	Q/µC	η_Q/mC mol^{-1} L	$[Zn^{2+}]$/nmol L^{-1}
1	$5 \times \times 10^6$	20	44.8	0.151	0.124	0.244
	$1 \times \times 10^7$	40	79.6	0.269	0.124	0.217
2	$5 \times \times 10^6$	30	48.0	0.170	0.124	0.275
	$1 \times \times 10^7$	60	96.8	0.336	0.124	0.271
3	$5 \times \times 10^6$	30	39.8	0.125	0.099	0.254
	$1 \times \times 10^7$	60	80.3	0.253	0.099	0.257
					Average	**0.25**
					σ	**0.02**

Additional factors not considered in this estimate include presence of weaker binding sites for which no accurate affinity data are available – these would be expected to decrease $[Zn^{2+}]$ – and the effects of our somewhat higher ionic strength, which would increase $[Zn^{2+}]$ very slightly. The significantly lower $[Zn^{2+}]$ determined by AGNES may, thus, largely reflect the effect of weaker additional binding sites.

The concentration value that we have determined in FBS ($[Zn^{2+}] = 0.25$ nmol L^{-1}) is an order of magnitude lower than that for the simple synthetic system with 600 µM BSA. This is the case even though the BSA concentration in FBS is typically lower [25] (about 350 µµmol L^{-1}), and total zinc is higher (>40 µµmol L^{-1}; this work). However, serum contains a plethora of other molecules with physiologically relevant zinc-binding ability, for example histidine-rich glycoprotein [79].

Our results compare favourably with related literature data. An early study using an enzymatic assay found $[Zn^{2+}] \approx 0.2$ nmol L^{-1} in equine blood plasma [80]. An approach using dialysis and atomic absorption spectrometry gave 0.141 nmol L^{-1} in bovine plasma [81]. More recent studies used a variety of fluorescent zinc sensors [30,31,35–37,41]. Values between 1 and 6 nmol L^{-1} free Zn^{2+} were found in a range of cell culture media with varying amounts of BSA (0.5%), FBS (5 or 10%) or horse serum (5%) added [37]. In rat plasma, a value of 1–3 nmol L^{-1} was inferred from measurements using the dye ZnAF-2. For 100% FBS, a value of ca. 0.75 nmol L^{-1} has been determined using FluoZin-3 [31]. Assays using Zinpyr-1 found 0.1 nmol L^{-1} free Zn^{2+} in porcine serum [41] and values ranging between 0.09 and 0.42 nmol L^{-1} in 154 sera from healthy human donors [30]. In one of our labs, we found previously that FluoZin-3 cannot report accurately on free Zn^{2+} in presence of 600 µµmol L^{-1} BSA or in neat FBS [25], because the probe bound to albumin, affecting both Zn^{2+}-dependent equilibria and fluorescence signals. This experience is in keeping with observations reported in some of the above studies [30,36], and also chimes with related work exploring the effects of proteins and small molecules on zinc-responsive dyes [24,28]. As a consequence, calibration of metal-responsive dyes in neat plasma or serum is recognised to have remained problematic [21]. Some of these problems can be circumvented by working at higher dilutions; for example, Alker et al. have carried out reliable measurements with 2% plasma [30]. It is satisfying to observe, and makes sense in biological terms, that their value for human plasma and our value for FBS have the same order of magnitude. Going forward, studying the same system with these two complementary approaches should serve to validate such measurements.

5. Conclusions

It has been emphasized that free Zn concentrations are, by far, more relevant in terms of zinc effects on cells [29,37], but absolute quantitation has remained challenging [21,31]. The electrochemical approach developed here offers a safe and complementary way of measurement, since it measures the free Zn concentration within the sample solution with minimal physical or chemical distortion, provided that the volume

of the sample is high enough to neglect speciation changes due to the Zn accumulated in the amalgam during the deposition step. However, though robust, it does not provide rapid access to [Zn^{2+}] or would not (yet) be suitable in a clinical context, but – with the aid of a Nafion coat – has the advantage of not being affected by interactions with complex media, and thus can, in principle, be applied to neat biological fluids with a minimum of sample manipulation.

We therefore propose that AGNES measurements, such as those developed here, may not only pave the way to addressing biological questions regarding processes where [Zn^{2+}] in extracellular media plays major roles (e.g. blood clotting [5,40]), but may also offer an independent method to calibrate the response of fluorescent dyes in other biological fluids of interest.

CRediT authorship contribution statement

Lucía López-Solís: Investigation, Methodology, Writing – original draft. **Encarna Companys:** Methodology, Writing – review & editing. **Jaume Puy:** Conceptualization, Writing – review & editing. **Claudia A. Blindauer:** Conceptualization, Writing – review & editing. **Josep Galceran:** Conceptualization, Writing – original draft.

Declaration of competing interest

The authors declare the following financial interests/personal relationships which may be considered as potential competing interests: Josep Galceran reports financial support was provided by Spanish Ministry of Science and Innovation. Jaume Puy and Encarna Companys reports financial support was provided by Spanish Ministry of Science and Innovation. Lucia Lopez-Solis reports financial support was provided by Horizon 2020. Claudia A. Blindauer reports financial support was provided by Leverhulme Trust.

Data availability

Data will be made available on request.

Acknowledgments

Support from the Spanish Ministry of Science and Innovation MCIN/AEI/10.13039/501100011033 is gratefully acknowledged (projects PID2019-107033GB-C21 and PID2020-117910GB-C21). This project has received funding from the European Union's H2020 research and innovation programme under Marie Sklodowska-Curie grant agreement No 801586. CAB thanks the Leverhulme Trust (RPG-2017-214) for support.

Appendix A. Supplementary data

Supplementary data to this article can be found online at https://doi.org/10.1016/j.aca.2022.340195.

References

[1] Y. Valasatava, A. Rosato, N. Furnham, J.M. Thornton, C. Andreini, To what extent do structural changes in catalytic metal sites affect enzyme function? J. Inorg. Biochem. 179 (2018) 40–53.
[2] C. Andreini, L. Banci, I. Bertini, A. Rosato, Counting the zinc-proteins encoded in the human genome, J. Proteome Res. 5 (1) (2006) 196–201.
[3] J.C. King, Zinc: an essential but elusive nutrient, Am. J. Clin. Nutr. 94 (2) (2011) 679S–684S.
[4] J.F. Seeler, A. Sharma, N.J. Zaluzec, R. Bleher, B. Lai, E.G. Schultz, B.M. Hoffman, C. LaBonne, T.K. Woodruff, T.V. O'Halloran, Metal ion fluxes controlling amphibian fertilization, Nat. Chem. 13 (7) (2021) 683–691.
[5] S. Arya, A.J. Gourley, J.C. Penedo, C.A. Blindauer, A.J. Stewart, Fatty acids may influence insulin dynamics through modulation of albumin-Zn2+ interactions, Bioessays 43 (12) (2021) 9.
[6] I. Wessels, M. Maywald, L. Rink, Zinc as a gatekeeper of immune function, Nutrients 9 (12) (2017) 44.
[7] Z.R. Lonergan, E.P. Skaar, Nutrient zinc at the host-pathogen interface, Trends Biochem. Sci. 44 (12) (2019) 1041–1056.
[8] T.T. Vu, J.C. Fredenburgh, J.I. Weitz, Zinc: an important cofactor in haemostasis and thrombosis, Thromb. Haemostasis 109 (3) (2013) 421–430.
[9] A. Takeda, H. Tamano, The impact of synaptic Zn(2+) dynamics on cognition and its decline, Int. J. Mol. Sci. 18 (11) (2017).
[10] A. Fukunaka, Y. Fujitani, Role of zinc homeostasis in the pathogenesis of diabetes and obesity, Int. J. Mol. Sci. 19 (2) (2018).
[11] C.A. Blindauer, Advances in the molecular understanding of biological zinc transport, Chem. Commun. 51 (22) (2015) 4544–4563.
[12] T. Kambe, K.M. Taylor, D. Fu, Zinc transporters and their functional integration in mammalian cells, J. Biol. Chem. 296 (2021) 27.
[13] N. Levaot, M. Hershfinkel, How cellular Zn2+ signaling drives physiological functions, Cell Calcium 75 (2018) 53–63.
[14] W. Maret, Zinc in cellular regulation: the nature and significance of "zinc signals", Int. J. Mol. Sci. 18 (11) (2017) 12.
[15] T. Fukada, S. Yamasaki, K. Nishida, M. Murakami, T. Hirano, Zinc homeostasis and signaling in health and diseases: zinc signaling, J. Biol. Inorg. Chem. 16 (7) (2011) 1123–1134.
[16] C.M. Elitt, C.J. Fahrni, P.A. Rosenberg, Zinc homeostasis and zinc signaling in white matter development and injury, Neurosci. Lett. 707 (2019), 134247.
[17] E. Tomat, S.J. Lippard, Imaging mobile zinc in biology, Curr. Opin. Chem. Biol. 14 (2) (2010) 225–230.
[18] M.R. Karim, D.H. Petering, Newport Green, a fluorescent sensor of weakly bound cellular Zn2+: competition with proteome for Zn2+, Metallomics 8 (2) (2016) 201–210.
[19] I. Marszalek, W. Goch, W. Bal, Ternary Zn(II) complexes of fluorescent zinc probes zinpyr-1 and zinbo-5 with the low molecular weight component of exchangeable cellular zinc pool, Inorg. Chem. 58 (21) (2019) 14741–14751.
[20] E.P.S. Pratt, L.J. Damon, K.J. Anson, A.E. Palmer, Tools and techniques for illuminating the cell biology of zinc, Biochim. Biophys. Acta-Mol. Cell Res. 1868 (1) (2021) 12.
[21] W. Maret, Analyzing free zinc(II) ion concentrations in cell biology with fluorescent chelating molecules, Metallomics 7 (2) (2015) 202–211.
[22] P. Chabosseau, J. Woodier, R. Cheung, G.A. Rutter, Sensors for measuring subcellular zinc pools, Metallomics 10 (2) (2018) 229–239.
[23] L. Fang, M. Watkinson, Subcellular localised small molecule fluorescent probes to image mobile Zn2+, Chem. Sci. 11 (42) (2020) 11366–11379.
[24] A.B. Nowakowski, J.W. Meeusen, H. Menden, H. Tomasiewicz, D.H. Petering, Chemical biological properties of zinc sensors TSQ and zinquin: formation of sensor-Zn-protein adducts versus Zn(Sensor)(2) complexes, Inorg. Chem. 54 (24) (2015) 11637–11647.
[25] J.P.C. Coverdale, J.P. Barnett, A.H. Adamu, E.J. Griffiths, A.J. Stewart, C. A. Blindauer, A metalloproteomic analysis of interactions between plasma proteins and zinc: elevated fatty acid levels affect zinc distribution, Metallomics 11 (11) (2019) 1805–1819.
[26] M.R. Karim, D.H. Petering, Detection of Zn2+ release in nitric oxide treated cells and proteome: dependence on fluorescent sensor and proteomic sulfhydryl groups, Metallomics 9 (4) (2017) 391–401.
[27] A. Staszewska, E. Kurowska, W. Bal, Ternary complex formation and competition quench fluorescence of ZnAF family zinc sensors, Metallomics 5 (11) (2013) 1483–1490.
[28] I. Marszalek, W. Goch, W. Bal, Ternary Zn(II) complexes of FluoZin-3 and the low molecular weight component of the exchangeable cellular zinc pool, Inorg. Chem. 57 (16) (2018) 9826–9838.
[29] H. Haase, S. Hebel, G. Engelhardt, L. Rink, The biochemical effects of extracellular Zn2+ and other metal ions are severely affected by their speciation in cell culture media, Metallomics 7 (1) (2015) 97–106.
[30] W. Alker, T. Schwerdtle, L. Schomburg, H. Haase, A zinpyr-1-based fluorimetric microassay for free zinc in human serum, Int. J. Mol. Sci. 20 (16) (2019).
[31] J. Ollig, V. Kloubert, I. Weßels, H. Haase, L. Rink, Parameters influencing zinc in experimental systems in vivo and in vitro, Metals 6 (3) (2016) 71.
[32] E.L. Giroux, R.I. Henkin, Competition for zinc among serum-albumin and amino-acids, Biochim. Biophys. Acta 273 (1) (1972) 64. &.
[33] D.L. Bloxam, J.C.Y. Tan, C.E. Parkinson, Non-protein bound zinc concentration in human-plasma and amniotic-fluid measured by ultrafiltration, Clin. Chim. Acta 144 (2–3) (1984) 81–93.
[34] J.W. Foote, H.T. Delves, Determination of non-protein-bound zinc in human serum using ultrafiltration and atomic-absorption spectrometry with electrothermal atomization, Analyst 113 (6) (1988) 911–915.
[35] E. Kelly, J. Mathew, J.E. Kohler, A.L. Blass, A.D. Soybel, Hemorrhagic shock and surgical stress alter distribution of labile zinc within high- and low-molecular-weight plasma fractions, Shock 38 (3) (2012) 314–319.
[36] E. Kelly, J. Mathew, J.E. Kohler, A.L. Blass, D.I. Soybel, Redistribution of labile plasma zinc during mild surgical stress in the rat, Transl. Res. 157 (3) (2011) 139–149.
[37] R.A. Bozym, F. Chimienti, L.J. Giblin, G.W. Gross, I. Korichneva, Y.A. Li, S. Libert, W. Maret, M. Parviz, C.J. Frederickson, R.B. Thompson, Free zinc ions outside a narrow concentration range are toxic to a variety of cells in vitro, Exp. Biol. Med. 235 (6) (2010) 741–750.
[38] W. Lin, J. Chai, J. Love, D. Fu, Selective electrodiffusion of zinc ions in a zrt-, Irt-like protein, ZIPB, J. Biol. Chem. 285 (50) (2010) 39013–39020.
[39] W. Maret, Zinc in pancreatic islet biology, insulin sensitivity, and diabetes, Prev. Nutr. Food Sci. 22 (1) (2017) 1–8.
[40] A.I.S. Sobczak, K.G.H. Katundu, F.A. Phoenix, S. Khazaipoul, R.T. Yu, F. Lampiao, F. Stefanowicz, C.A. Blindauer, S.J. Pitt, T.K. Smith, R.A. Ajjan, A.J. Stewart,

Albumin-mediated alteration of plasma zinc speciation by fatty acids modulates blood clotting in type-2 diabetes, Chem. Sci. 12 (11) (2021) 4079–4093.
[41] J. Hoeger, T.P. Simon, S. Doemming, C. Thiele, G. Marx, T. Schuerholz, H. Haase, Alterations in zinc binding capacity, free zinc levels and total serum zinc in a porcine model of sepsis, Biometals 28 (4) (2015) 693–700.
[42] J. Galceran, E. Companys, J. Puy, J. Cecília, J.L. Garcés, AGNES: a new electroanalytical technique for measuring free metal ion concentration, J. Electroanal. Chem. 566 (2004) 95–109.
[43] E. Companys, J. Galceran, J.P. Pinheiro, J. Puy, P. Salaün, A review on electrochemical methods for trace metal speciation in environmental media, Curr. Opin. Electrochem. 3 (1) (2017) 144–162.
[44] E. Companys, J. Puy, J. Galceran, Humic acid complexation to Zn and Cd determined with the new electroanalytical technique AGNES, Environ. Chem. 4 (2007) 347–354.
[45] W.B. Chen, C. Gueguen, D.S. Smith, J. Galceran, J. Puy, E. Companys, Metal (Pb, Cd, and Zn) binding to diverse organic matter samples and implications for speciation modeling, Environ. Sci. Technol. 52 (7) (2018) 4163–4172.
[46] E. Companys, M. Naval-Sanchez, N. Martinez-Micaelo, J. Puy, J. Galceran, Measurement of free zinc concentration in wine with AGNES, J. Agric. Food Chem. 56 (18) (2008) 8296–8302.
[47] M. Lao, E. Companys, L. Weng, J. Puy, J. Galceran, Speciation of Zn, Fe, Ca and Mg in wine with the donnan membrane technique, Food Chem. 239 (2018) 1143–1150.
[48] C. David, J. Galceran, C. Rey-Castro, J. Puy, E. Companys, J. Salvador, J. Monné, R. Wallace, A. Vakourov, Dissolution kinetics and solubility of ZnO nanoparticles followed by AGNES, J. Phys. Chem. C 116 (21) (2012) 11758–11767.
[49] C.A. David, J. Galceran, F. Quattrini, J. Puy, C. Rey-Castro, Dissolution and phosphate-induced transformation of ZnO nanoparticles in synthetic saliva probed by AGNES without previous solid-liquid separation. Comparison with UF-ICP-MS, Environ. Sci. Technol. 53 (2019) 3823–3831.
[50] H.B.C. Pearson, J. Galceran, E. Companys, C. Braungardt, P. Worsfold, J. Puy, S. Comber, Absence of gradients and nernstian equilibrium stripping (AGNES) for the determination of [Zn2+] in estuarine waters, Anal. Chim. Acta 912 (2016) 32–40.
[51] K. Rosales-Segovia, J. Sans-Duñó, E. Companys, J. Puy, B. Alcalde, E. Antico, C. Fontas, J. Galceran, Effective concentration signature of Zn in a natural water derived from various speciation techniques, Sci. Total Environ. (2021), 151201 in press.
[52] D. Chito, L. Weng, J. Galceran, E. Companys, J. Puy, W.H. van Riemsdijk, H.P. van Leeuwen, Determination of free Zn^{2+} concentration in synthetic and natural samples with AGNES (absence of gradients and nernstian equilibrium stripping) and DMT (donnan membrane technique), Sci. Total Environ. 421–422 (2012) 238–244.
[53] J.C. Vidal, G. Cepria, J.R. Castillo, Models for studying the binding-capacity of albumin to zinc by stripping voltammetry, Anal. Chim. Acta 259 (1) (1992) 129–138.
[54] L.S. Rocha, E. Companys, J. Galceran, H.M. Carapuca, J.P. Pinheiro, Evaluation of thin mercury film rotating disc electrode to perform Absence of Gradients and Nernstian Equilibrium Stripping (AGNES) measurements, Talanta 80 (2010) 1881–1887.
[55] E. Rotureau, P. Pla-Vilanova, J. Galceran, E. Companys, J.P. Pinheiro, Towards improving the electroanalytical speciation analysis of indium, Anal. Chim. Acta 1052 (2019) 57–64.
[56] J. Galceran, M. Lao, C. David, E. Companys, C. Rey-Castro, J. Salvador, J. Puy, The impact of electrodic adsorption on Zn, Cd or Pb speciation measurements with AGNES, J. Electroanal. Chem. 722–723 (2014) 110–118.
[57] M.H. Tehrani, E. Companys, A. Dago, J. Puy, J. Galceran, Free Indium concentration determined with AGNES, Sci. Total Environ. 612 (2018) 269–275.
[58] E. Companys, J. Cecília, G. Codina, J. Puy, J. Galceran, Determination of the concentration of free Zn^{2+} with AGNES using different strategies to reduce the deposition time, J. Electroanal. Chem. 576 (1) (2005) 21–32.
[59] C. Parat, L. Authier, D. Aguilar, E. Companys, J. Puy, J. Galceran, M. Potin-Gautier, Direct determination of free metal concentration by implementing stripping chronopotentiometry as second stage of AGNES, Analyst 136 (2011) 4337–4343.
[60] T. Peters, All about Albumin; Biochemistry, Genetics and Medical Applications, Academic Press, San Diego (CA), 1995.
[61] M. Rukgauer, J. Klein, J.D. KruseJarres, Reference values for the trace elements copper, manganese, selenium, and zinc in the serum/plasma of children, adolescents, and adults, J. Trace Elem. Med. Biol. 11 (2) (1997) 92–98.
[62] J. Lu, A.J. Stewart, P.J. Sadler, T.J.T. Pinheiro, C.A. Blindauer, Albumin as a zinc carrier: properties of its high-affinity zinc-binding site, Biochem. Soc. Trans. 36 (2008) 1317–1321.
[63] W. Bal, M. Sokolowska, E. Kurowska, P. Faller, Binding of transition metal ions to albumin: sites, affinities and rates, Biochim. Biophys. Acta-Gen. Subj. 1830 (12) (2013) 5444–5455.
[64] L.S. Rocha, J. Galceran, J. Puy, J.P. Pinheiro, Determination of the free metal ion concentration using AGNES implemented with environmentally friendly bismuth film electrodes, Anal. Chem. 87 (12) (2015) 6071–6078.
[65] L.S. Rocha, J.P. Pinheiro, H.M. Carapuca, Ion-exchange voltammetry with nafion/poly(sodium 4-styrenesulfonate) mixed coatings on mercury film electrodes: characterization studies and application to the determination of trace metals, Langmuir 22 (19) (2006) 8241–8247.
[66] B. Hoyer, N. Jensen, Signal stability of nafion-coated thin mercury film electrodes for stripping voltammetry, Talanta 41 (3) (1994) 449–453.
[67] M.L. Tercier, J. Buffle, Antifouling membrane-covered voltammetric microsensor for in- situ measurements in natural-waters, Anal. Chem. 68 (1996) 3670–3678.
[68] M.E.R. Dam, K.H. Schroder, Mercury film electrodes coated with negatively charged polymer films in speciation studies of trace amounts of lead, Electroanalysis 8 (11) (1996) 1040–1050.
[69] M.P. Hurst, K.W. Bruland, The use of Nafion-coated thin mercury film electrodes for the determination of the dissolved copper speciation in estuarine water, Anal. Chim. Acta 546 (1) (2005) 68–78.
[70] S. Andrade, J. Moffett, J.A. Correa, Distribution of dissolved species and suspended particulate copper in an intertidal ecosystem affected by copper mine tailings in Northern Chile, Mar. Chem. 101 (3–4) (2006) 203–212.
[71] L.S. Rocha, H.M. Carapuca, Ion-exchange voltammetry of dopamine at Nafion-coated glassy carbon electrodes: quantitative features of ion-exchange partition and reassessment on the oxidation mechanism of dopamine in the presence of excess ascorbic acid, Bioelectrochemistry 69 (2) (2006) 258–266.
[72] E. Leppanen, A. Peltonen, J. Seitsonen, J. Koskinen, T. Laurila, Effect of thickness and additional elements on the filtering properties of a thin Nafion layer, J. Electroanal. Chem. 843 (2019) 12–21.
[73] A.K. Covington, R.A. Robinson, References standards for electrometric determination, with ion-selective electrodes, of potassium and calcium in blood serum, Anal. Chim. Acta 78 (1) (1975) 219–223.
[74] M. Jayaraman, P.M. Buck, A.A. Ignatius, K.R. King, W. Wang, Agitation-induced aggregation and subvisible particulate formation in model proteins, Eur. J. Pharm. Biopharm. : Off. J. Arbeitsgemeinschaft Pharm. Verfahrenstech. E.V. 87 (2) (2014) 299–309.
[75] J.J. Lin, J.D. Meyer, J.F. Carpenter, M.S. Manning, Stability of human serum albumin during bioprocessing: denaturation and aggregation during processing of albumin paste, Pharm. Res. (N. Y.) 17 (4) (2000) 391–396.
[76] E. Ohyoshi, Y. Hamada, K. Nakata, S. Kohata, The interaction between human and bovine serum albumin and zinc studied by a competitive spectrophotometry, J. Inorg. Biochem. 75 (3) (1999) 213–218.
[77] J. Masuoka, P. Saltman, Zinc(II) and copper(II) binding to serum albumin. A comparative study of dog, bovine, and human albumin, J. Biol. Chem. 269 (41) (1994) 25557–25561.
[78] J. Lu, A.J. Stewart, D. Sleep, P.J. Sadler, T.J.T. Pinheiro, C.A. Blindauer, A molecular mechanism for modulating plasma Zn speciation by fatty acids, J. Am. Chem. Soc. 134 (3) (2012) 1454–1457.
[79] O. Kassaar, U. Schwarz-Linek, C.A. Blindauer, A.J. Stewart, Plasma free fatty acid levels influence Zn2+-dependent histidine-rich glycoprotein-heparin interactions via an allosteric switch on serum albumin, J. Thromb. Haemostasis 13 (1) (2015) 101–110.
[80] G.R. Magneson, J.M. Puvathingal, W.J. Ray Jr., The concentrations of free Mg2+ and free Zn2+ in equine blood plasma, J. Biol. Chem. 262 (23) (1987) 11140–11148.
[81] P. Zhang, J.C. Allen, A novel dialysis procedure measuring free Zn2+ in bovine milk and plasma, J. Nutr. 125 (7) (1995) 1904–1910.